CLINICS

CLINICAL SCIENCE

Evaluation of pulmonary sequestration with multidetector computed tomography angiography in a select cohort of patients: A retrospective study

Qihua Long,[I,#] Yunfei Zha,[I,#] Zhigang Yang[II,*]

[I]Renmin Hospital of Wuhan University, Department of Radiology, Wuhan, China. [II]Sichuan University, West China Hospital, Department of Radiology, Chengdu, China.

OBJECTIVES: This study aimed to evaluate the role of multidetector computed tomography angiography in diagnosing patients with pulmonary sequestration.

METHODS: We retrospectively analyzed the computed tomography studies and clinical materials of 43 patients who had undergone preoperative multidetector computed tomography angiography in our hospital and had pathologically proven pulmonary sequestration. Each examination of pulmonary sequestration was reviewed for type, location, parenchymal changes, arterial supply and venous drainage on two-dimensional and three-dimensional computed tomography images.

RESULTS: Multidetector computed tomography successfully detected all pulmonary sequestrations in the 43 patients (100%). This included 40 patients (93.0%) with intralobar sequestration and 3 patients (7.0%) with extralobar sequestration. The locations of pulmonary sequestration were left lower lobe (28 cases, 70% of intralobar sequestrations), right lower lobe (12 cases, 30% of intralobar sequestrations) and costodiaphragmatic sulcus (3 cases). Cases of sequestered lung presented as mass lesions (37.2%), cystic lesions (32.6%), pneumonic lesions (16.3%), cavitary lesions (9.3%) and bronchiectasis (4.6%). The angioarchitecture of pulmonary sequestration, including feeding arteries from the thoracic aorta (86.1%), celiac truck (9.3%), abdominal aorta (2.3%) and left gastric artery (2.3%) and venous drainage into inferior pulmonary veins (86.0%) and the azygos vein system (14.0%), was visualized on multidetector computed tomography. Finally, the multidetector computed tomography angiography results of the sequestered lungs and angioarchitectures were surgically confirmed in all the patients.

CONCLUSIONS: As a noninvasive modality, multidetector computed tomography angiography is helpful for making diagnostic decisions regarding pulmonary sequestration with high confidence and for visualizing the related parenchymal characteristics, arterial supply, and venous drainage features to help plan surgical strategies.

KEYWORDS: Pulmonary Sequestration; Computed Tomography; Congenital Anomalies.

Long Q, Zha Y, Yang Z. Evaluation of pulmonary sequestration with multidetector computed tomography angiography in a select cohort of patients: A retrospective study. Clinics. 2016;71(7):392-398

Received for publication on February 2, 2016; **First review completed on** April 8, 2016; **Accepted for publication on** April 14, 2016

*Corresponding author. E-mail: yangzg666@163.com

[#]Contributed equally to this work

INTRODUCTION

Pulmonary sequestration is characterized by an area of dysplastic and nonfunctional lung tissue that receives its blood supply from aberrant systemic arteries and is not in normal continuity with the tracheobronchial tree (1). It is usually classified as either intralobar sequestration (ILS), which is located within a lung lobe and shares the visceral pleura with the corresponding lung lobe, or extralobar sequestration (ELS), which is a separate mass of lung parenchyma enclosed entirely by a separate pleural envelope (2). Intralobar sequestration accounts for 75% of pulmonary sequestration, while ELS constitutes the remaining 25%. Although ILS almost always occurs within the lower lobe (98%) and more often in the left lung (55%), ELS is typically found in the posterior costodiaphragmatic sulcus (1,3). Previous studies have assessed the sensitivity and specificity of computed tomography (CT) compared with digital subtraction angiography (DSA); however, most published reports have evaluated only a small number of cases. Therefore, the aim of the current study was to evaluate the role of multidetector computed tomography (MDCT)

No potential conflict of interest was reported.

DOI: 10.6061/clinics/2016(07)07

angiography in diagnosing pulmonary sequestration by analyzing the CT data of 43 patients with clinically proven pulmonary sequestration.

MATERIALS AND METHODS

Patients

The institutional review board of our institution approved the review of the data included in this retrospective study. Informed consent was waived, but we guaranteed protection of patient confidentiality. We used the information systems from our radiology, surgery and pathology departments to identify all consecutive patients between March 2010 and October 2015. The inclusion criteria were both preoperative MDCT angiography and pathologically proven pulmonary sequestration and the exclusion criterion was pulmonary sequestration diagnosed by an alternative technique. The final study cohort consisted of 43 patients (19 males and 24 females; mean age, 34.4 ± 14.5 [standard deviation, SD] years; range, 3–68 years). Among these individuals, 29 patients presented with cough or expectoration (20 patients had a productive cough), 11 patients presented with chest pain, 9 patients presented with fever, 7 patients presented with hemoptysis and 1 patient presented with night sweats. In other words, 17 patients had just one symptom, 18 patients had more than one symptom and the remaining 8 patients were asymptomatic and their pulmonary sequestration was accidentally discovered on routine physical examination. All patients underwent either video-assisted thoracoscopic lobectomy (n=26, 60%) or lobectomy via conventional thoracotomy (n=17 40%) to definitively diagnose their disease. The mean time interval between MDCT and surgery was 11.6 ± 4.3 [SD] days.

Scanning parameters

All CT angiographies were performed using either a dual source CT scanner (DSCT, n=28, 65%; Somatom Definition, Siemens Healthcare, Forchheim, Germany) or a 64-slice MDCT (64-MDCT, n=15, 35%; Brilliance 64, Philips Medical Systems, Eindhoven, Netherlands). All MDCT images were obtained while the patients were in a supine position and holding their breath. The parameters for the DSCT and 64-MDCT included 0.6 mm and 0.625 mm of collimation, 0.28 s and 0.42 s of rotation time, 100 kV and 120 kV of kilovoltage and 150 mAs and 180 mAs of tube current, respectively, and a helical pitch equivalent of 0.9 was used for both scanners. Weight-based kilovoltage (70–100 kV) with a low-dose tube current (30–80 mAs) was used for the children. We administered a standard dose of 10% chloral hydrate (0.3 mL/kg, not to exceed 0.6 mL/kg) to the children who were noncooperative during examination. Enhanced MDCT angiography was performed in the children with a standard dose of 1.5 mL/kg (not to exceed 2 mL/kg) of nonionic contrast agent (iopamidol, 370 mg iodin/mL; Shanghai Bracco Pharmaceutical Company, Shanghai, China), and the adult patients were administered 60–80 mL of the contrast agent. Thereafter, 20–30 mL (10–20 mL for the children) of normal saline was administered through a 20-gauge (24-gauge for the children) needle into the antecubital vein. The contrast agent was injected at a rate of 1.2–2.5 mL/s using an automatic power injector (Stellant D Dual Syringe, Medrad, Indianola, PA, USA). When the concentration of contrast medium in the ascending aorta reached 100 Hu, the CT device automatically scanned the area of coverage extending from just above the level of the thoracic inlet, including the proximal aspect of the common carotid and subclavian arteries, to the level just above the renal arteries. The acquired image datasets were then transferred to a workstation (Siemens Syngo Studio Advanced, Siemens Medical Systems, Forchheim, Germany). For reconstructions, we used CT datasets with slice thicknesses of 0.6 mm and 0.625 mm for the DSCT and 64-MDCT, respectively. Image reconstruction was performed with a 512 × 512 matrix.

Imaging analysis

Two board-certified chest radiologists who were experienced in creating and interpreting two-dimensional (2D) and three-dimensional (3D) MDCT reconstructions independently reviewed the images. The reviewers were blinded to the results of other imaging studies, surgical findings, and pathologic characteristics. Any differences in the opinions of the radiologists were resolved by consensus. For the image review session, the cases were randomized so that the datasets were not reviewed consecutively for the same patient. For each case, each reviewer first interpreted the axial MDCT images, followed by the multiplanar reconstruction (MPR), maximum intensity projection (MIP), and volume rendering (VR) images. The oblique, sagittal, and coronal images were reconstructed and reviewed for all cases for MPR image evaluation. The VR images of the central airways, sequestered lungs, and vascular structures were reconstructed and reviewed as 3D images in real time. The images were rotated by the reviewers so that they could observe the central airways, sequestered lungs and anomalous vessels from any orientation.

Each patient was assessed for pulmonary sequestration after at least one artery originating from systemic circulation was identified by MDCT angiography. The location, subtype, lung sequestration status, and course of each anomalous vessel were evaluated using axial, MPR, MIP and VR images by adjusting the values of the translucency or slab thicknesses. Location was assessed and recorded using the standard nomenclature for lung lobes and segments. The sizes of the sequestered lungs and anomalous vessels were measured on the MPR images. The sizes of the anomalous vessels at their largest transverse diameters were measured and recorded. Each segmental bronchus of an involved lung was reconstructed using MPR and MIP images. Moreover, the accompanying abnormalities were also recorded.

Statistical analysis

The ages of the patients followed a normal distribution and were expressed as the mean, SD and range. Data were analyzed using the commercially available software package IBM SPSS (version 22, IBM, Armonk, NYC, USA). We compared differences between the feeding arteries associated with the two subtypes of pulmonary sequestration. The variables were expressed as cases (percentages) and tested using Fisher's exact test. The statistical tests were two-tailed, and p-values of less than 0.05 were considered statistically significant.

RESULTS

Subtypes and locations

All patients underwent surgical resection after MDCT angiography with subsequent histopathologic confirmation

Table 1 - Location and lesion details for 43 patients with pulmonary sequestration.

Locations/lesions	All patients (n=43)	ILS (n=40)	ELS (n=3)
Locations [n (%)]			
Left lower lobe	28 (65.1)	28 (70.0)	-
Right lower lobe	12 (27.9)	12 (30.0)	-
Left costodiaphragmatic sulcus	2	-	2
Right costodiaphragmatic sulcus	1	-	1*
Lesions [n (%)]			
Mass lesions	16 (37.2)	14 (35.0)	2 (66.7)
Cystic lesions	14 (32.6)	14 (35.0)	-
Pneumonic lesions	7 (16.3)	7 (17.5)	-
Cavitary lesions	4 (9.3)	4 (10.0)	-
Bronchiectasis	2 (4.6)	1	1

ILS = intralobar sequestration, ELS = extralobar sequestration
* = the patient with ELS and accompanying ILS.

of pulmonary sequestration. Both reviewers correctly diagnosed all subtypes and locations of pulmonary sequestration with high accuracy (100%). The final histopathologic diagnoses included ILS (n=40, 93.0%) and ELS (n=3, 7.0%). One patient with ELS in the right costodiaphragmatic sulcus had accompanying ILS in the right lower lobe. In 26 patients with ILS, the sequestrations were located in a single segment of lung and 14 patients had more than two segments involved. The locations, subtypes and lesions of the patients with pulmonary sequestrations are summarized in Table 1.

Lesions and accompanying abnormalities

The most common lesions of pulmonary sequestration were mass lesions (n=16, 37.2%; Figure 1), followed by cystic lesions (n=14, 32.6%). The mass lesions had a maximum diameter of 1.7–9.8 cm. There was mild enhancement in most mass lesions and the solid parts of cavitary lesions, while no

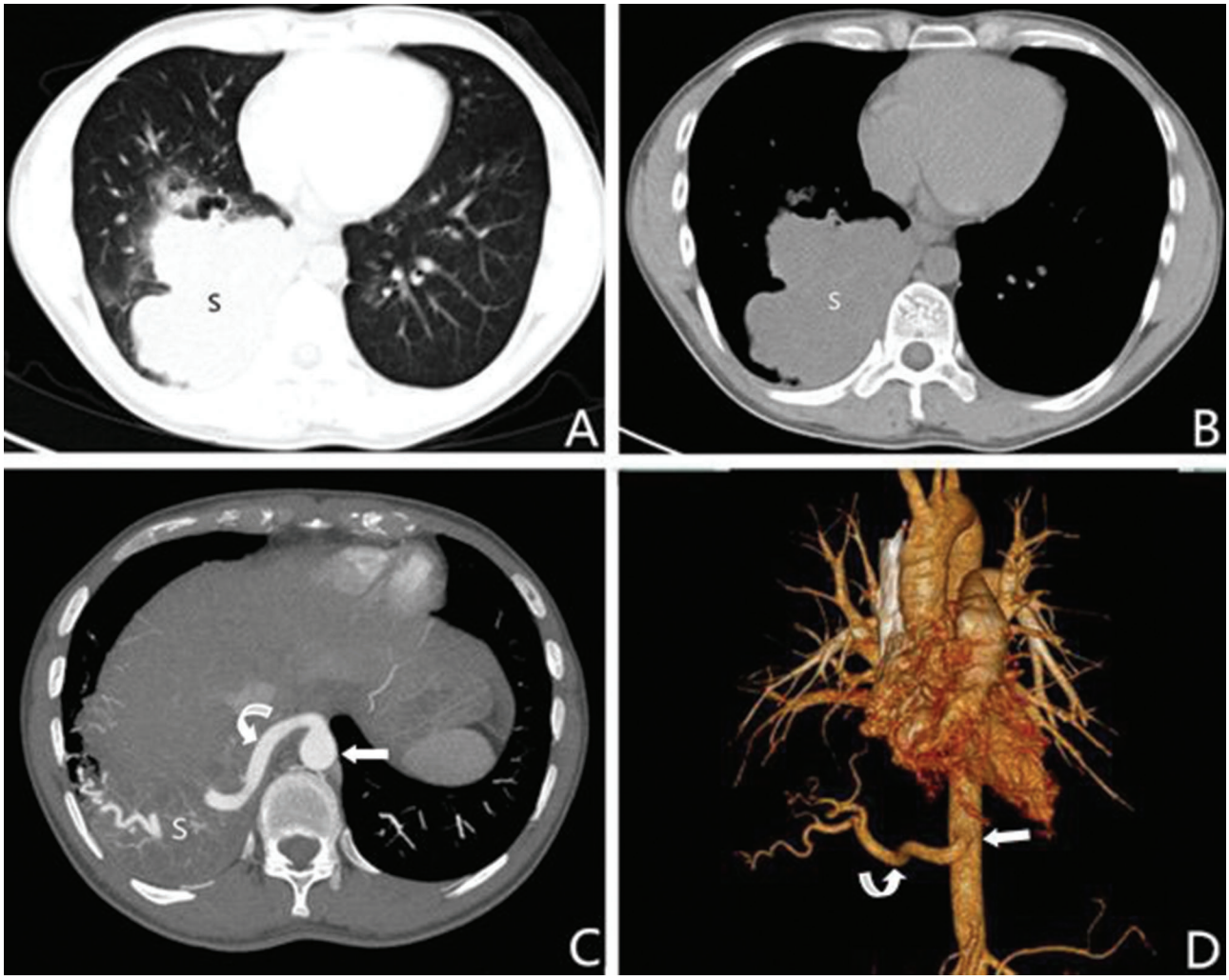

Figure 1 - A 32-year-old male with intralobar sequestration. A and B: Axial multidetector computed tomography images show a mass in the right lower lobe (S); C: An axial multidetector computed tomography image obtained at a level lower than A and B shows an aberrant artery (curved arrow) arising from the thoracic aorta (straight arrow) to the sequestered lung (S); D: A 3D multidetector computed tomography volume rendering image shows an aberrant artery (curved arrow) from the thoracic aorta (straight arrow) to the right lower lobe.

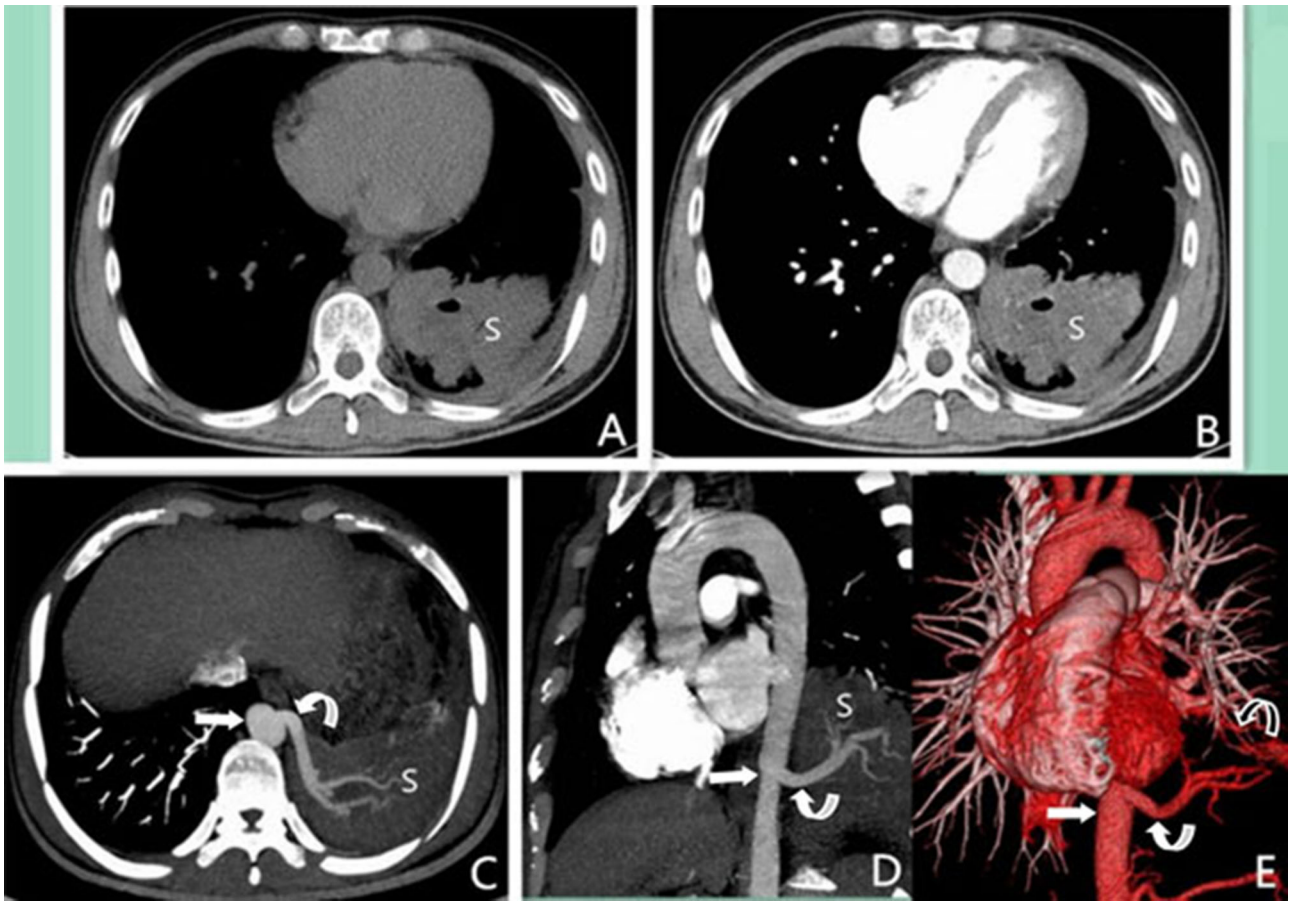

Figure 2 - A 33-year-old male with intralobar sequestration that was pathologically proven to be accompanied by *M. tuberculosis* infection. A and B: Axial multidetector computed tomography images show the lesion with a gas-fluid level in the left lower lobe (S). The lesion exhibited mild enhancement in the solid part and no enhancement in the cavity; C and D: Axial (obtained at a lower level than A and B) and sagittal maximum intensity projection images show the aberrant artery (curved arrow) arising from the thoracic aorta (straight arrow) to the sequestered lung (S); E: A 3D multidetector computed tomography volume rendering image shows an aberrant artery (curved arrow) arising from the thoracic aorta (straight arrow) and anomalous vein (curved arrow) via the left inferior pulmonary vein to the left atrium.

enhancement was observed in cystic lesions. The pathological results of one patient who had a cavitary lesion with a gas-fluid interface proved to be accompanied by a *Mycobacterium tuberculosis* infection (Figure 2). Three patients with mass lesions had obvious enhancement. Thirteen patients (30.2%) had lesions with calcification.

Except for the ILS patients who had pneumonic lesions and bronchiectasis as the only lesion, we identified accompanying lesions, including chronic pneumonic (n=16, 37.2% of ILS), bronchiectasis (n=5), bronchogenic cyst (n=5), emphysema (n=3), ventricular septal defect (n=2), and accessory spleen (n=2), in most patients. Accompanying pleural thickening and lymph node enlargement were each identified in 8 patients.

Angioarchitecture

All pulmonary sequestration patients were found to have associated anomalous feeding arteries and draining veins on MDCT images. Both reviewers correctly detected anomalous arteries and draining veins associated with pulmonary sequestration with high accuracy (100%). The anomalous arteries ranged in size from 0.2–1.2 cm, with an average of 0.5 cm. The feeding arteries and draining veins of the pulmonary sequestrations are summarized in Table 2. The feeding arteries most commonly originated from the thoracic aorta (n=37, 86.1%). All the feeding arteries of left-sided pulmonary sequestration came from the thoracic aorta. The pulmonary sequestrations on the right side were supplied by the thoracic aorta in 7 cases and by the abdominal aorta or its branches (Figure 3) in 6 cases. The draining veins reflowed into the left or right inferior pulmonary vein in 37 ILS patients (92.5%) and in the remaining ILS patients they reflowed into the azygos vein system. The patient who had ELS accompanying ILS had an artery from the celiac trunk to both the ILS and ELS and the ILS drained into the left atrium via the right inferior pulmonary vein, while the ELS drained into the right atrium via the hemiazygos vein.

As shown in Table 2, the differences in arterial supply from the thoracic aorta or from the celiac trunk between the ILS and the ELS cases were not considered statistically significant (p=0.370 and p=0.259, respectively).

DISCUSSION

Pulmonary sequestration, a rare pulmonary malformation that constitutes approximately 0.15–6.4% of all congenital

CLINICS 2016;71(7):392-398

Table 2 - Angioarchitecture details for 43 patients with pulmonary sequestration.

Angioarchitecture	All patients (n=43)	ILS (n=40)		ELS (n=3)		*p*- values
		Right	Left	Right	Left	ILS *vs.* ELS
Feeding arteries [n (%)]						
Thoracic aorta	37 (86.1)	7 (58.3)	28 (100)	-	2 (100)	0.370
Celiac trunk	4 (9.3)	3 (25.0)	-	1*	-	0.259
Left gastric artery	1 (2.3)	1	-	-	-	-
Abdominal aorta	1 (2.3)	1	-	-	-	-
Draining veins [n (%)]						
Left inferior pulmonary vein	25 (58.1)	-	25 (89.3)	-	-	-
Right inferior pulmonary vein	12 (27.9)	12	-	-	-	-
Azygos vein system	6 (14.0)	-	3 (10.7)	1*	2	-

ILS = intralobar sequestration, ELS = extralobar sequestration
* = The case with ELS and accompanying ILS with an anomalous artery from the celiac trunk and venous drainage into both the right inferior pulmonary vein and hemiazygos vein.

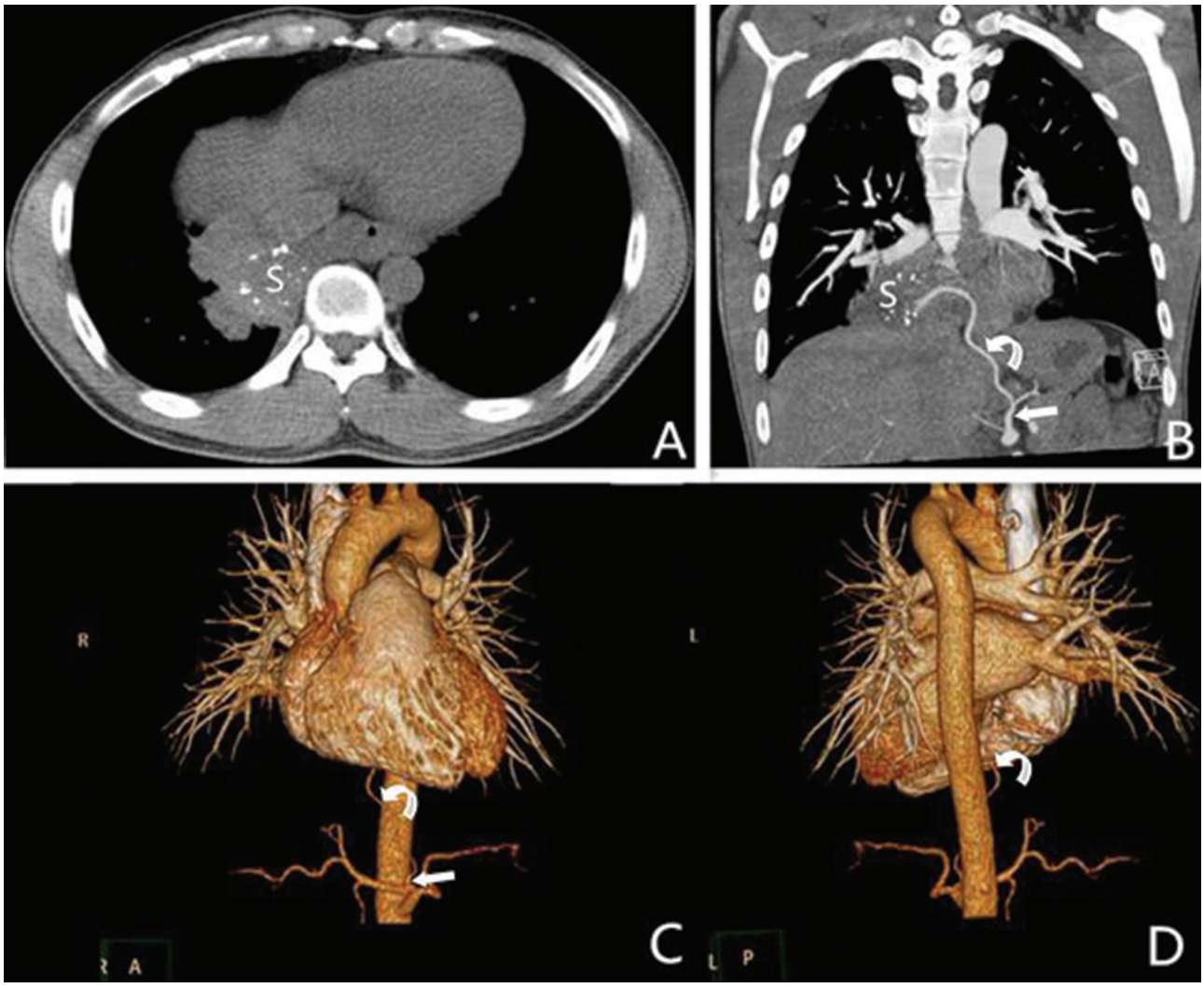

Figure 3 - A 30-year-old male with intralobar sequestration. A: Axial multidetector computed tomography images show a mass with calcification in the right lower lobe (S); B: A coronary multidetector computed tomography image shows an aberrant artery (curved arrow) arising from the left gastric artery (straight arrow) to the sequestered lung (S); C and D: Two 3D multidetector computed tomography volume rendering images show an aberrant artery (curved arrow) from the left gastric artery (straight arrow) to the right lower lobe.

pulmonary malformations, was initially described by Pryce in 1946 (3,4). The pathogenesis of ILS is controversial. In the past, ILS and ELS were described as having a shared embryologic origin in many medical publications (4). It is currently widely accepted that ILS is an acquired disease that is associated with bronchial obstruction, pneumonia and pleuritis. This could be partially attributed to the development of a systemic arterial supply secondary to angiogenic growth factors that are activated by recurrent infections. This would be the most plausible explanation for why ILS is found more frequently in adults and is rarely accompanied by other congenital diseases (5,6). Conversely, ELS is consistently accepted to be a truly congenital disease arising from the primitive foregut. This is consistent with its diagnosis, which typically occurs during the neonatal period and is usually association with other congenital anomalies (7).

Intralobar sequestration may be detected at any age and more than half of affected patients are diagnosed after the age of twenty. In contrast, ELS is more commonly diagnosed during the fetal and neonatal period and concurrent with diaphragmatic hernias, cardiac anomalies, or pulmonary hypoplasia (3,8). As previously described (7), ILS equally affects both males and females, but ELS has a male predominance. Some patients with pulmonary sequestration are asymptomatic and incidentally discovered. Recurrent episodes of pneumonia are the most common symptoms of patients with ILS because bronchial drainage does not proceed normally when bacteria have colonized a sequestered lung. Grossly, ILS usually has chronic inflammation due to recurrent infection, with fibrosis and cysts in the parenchyma and occasional adjacent pleural thickening with adhesions (9). However, ELS may appear normal on histology or only occasionally show chronic inflammation, while the cut surface may reveal cystic changes, fibrosis, or purulent secretions.

Our series contained 37 patients with ILS (92.5%) who were diagnosed over 20 years. Most of these patients had accompanying pneumonic lesions, pleural thickening and enlargement of the lymph nodes and some lesions with calcification were also found. In ILS, the lymphatic circulation tends to drain to lymph nodes adjacent to the thoracic aorta. All of the above may be evidence of ILS being an acquired disease. However, we had one patient with ELS accompanying ILS in our study and 2 patients with accompanying accessory spleen and ventricular septal defects, which may instead support a congenital pathogenesis of ILS.

Similar with Wei et al.'s (10) study, the most common lesions identified in our series were mass lesions on MDCT. There was mild enhancement in patients with mass lesions and in the solid parts of cavitary lesions. Moreover, one patient had a cavitary lesion on MDCT, and the lesion was pathologically proved to be accompanied by an *M. tuberculosis* infection. The tuberculosis was confined to the sequestered lung tissue owing to the lack of connection between the sequestered lung and the normal bronchial tree (11).

The majority of the aberrant arteries in ILS arise from the thoracic aorta (75%) or abdominal aorta (15–20%). However, they can also originate from other smaller arteries that branch from either of these vessels. The pulmonary veins usually provide venous drainage into the left atrium in ILS (12). Moreover, 80% of the sequestered lungs in patients with ELS are typically supplied by an anomalous artery that arises directly from the thoracic or abdominal aorta. The azygos vein system or superior vena cava provides systemic venous drainage into the right atrium (1,7). The diagnosis of pulmonary sequestration traditionally requires DSA to identify the aberrant arteries that feed the sequestered lung (13). Although DSA is capable of identifying the aberrant arterial supply of a sequestered lung, it is invasive, requires hospitalization and does not provide sufficient information about pulmonary structure. At present, non-invasive imaging techniques, including MDCT, magnetic resonance imaging (MRI) and color Doppler ultrasonography, are also suitable diagnostics for pulmonary sequestration because of their capacity to both show a sequestered lung with anatomic localization and to reveal vessels. Particularly, MDCT has been proven to be equally effective to DSA and is regarded as a safer alternative, which can also overcome some limitations of MRI and ultrasound. Multidetector CT is not only capable of clearly identifying the angioarchitecture of pulmonary sequestration but also simultaneously yields the maximum information about parenchymal changes in a single examination when combined with advanced post-processing techniques (14). There are two principle objectives of MDCT angiography for the investigation of a suspected case of pulmonary sequestration: 1) to confirm the presence of an anomalous systemic arterial supply to the sequestered lung and 2) to distinguish pulmonary sequestration from other lung opacities (13). The ability to rotate 3D VR images and display them in any orientation is helpful in discerning the relationships that exist within aberrant angioarchitecture (15). These advantages of MDCT arise from its faster scanning and improved volume acquisition (16). In light of these advantages, MDCT has the potential to become a first-line examination for the preoperative assessment of pulmonary sequestration. In our study, MDCT angiography successfully delineated the origins and courses of the anomalous systemic arteries and venous drainage systems in all cases. The feeding arteries most commonly originated from the thoracic aorta. Indeed, our study showed a greater percentage of this type of origination than a study reported by Savic et al. (3), which may have been due to the limited number of samples. All the feeding arteries of pulmonary sequestration that were observed on the left side were from the thoracic aorta. The majority of the patients with right-sided pulmonary sequestration had feeding arteries that originated from the abdominal aorta or its branches. The draining vein reflowed into the inferior pulmonary vein in 37 patients (86.0%), which was a higher percentage than that reported by Yue et al.'s (17) but a lower percentage than reported by Savic et al. (3). The differences between ILS and ELS supplied by the celiac trunk or from the thoracic aorta were not considered to be statistically significant.

Surgical resection is the conventional standard treatment for both symptomatic and asymptomatic patients with pulmonary sequestration to prevent possible infection, congestive heart failure, and hemoptysis (18), but its value is debatable in asymptomatic patients (19). Nevertheless, most patients with pulmonary sequestration require a lobectomy, or at least a segmentectomy, of the involved lung, which are usually performed via conventional thoracotomy or video-assisted thoracoscopic resection (20). Recently, interventional treatment has emerged as a minimally invasive surgical alternative to lobectomy, especially in

neonates and children (21,22). An essential requirement for surgery is to identify and control aberrant angioarchitecture. Careful preoperative identification of systemic arterial supply and venous drainage from a pulmonary sequestration is necessary to avoid hemorrhage during surgery (23). MDCT information, including locations, morphological features and angioarchitectures of pulmonary sequestrations, is helpful for making preoperative decisions. In summary, MDCT angiography can be used to accurately identify the systemic arterial supply and drainage veins of a pulmonary sequestration when compared with pathological and surgical findings. In particular, this method yielded the maximum information for visualizing lung abnormalities, airways changes and small and tortuous vessels and should contribute to the development of surgical strategies.

AUTHOR CONTRIBUTIONS

Long Q and Zha Y prepared Tables 1-2 and Figures 1-3 and wrote the main manuscript text. All authors reviewed the manuscript, study concepts and design. Yang Z is the guarantor of the integrity of the entire study and also performed manuscript revision/review and final version approval.

REFERENCES

1. Mendeloff EN. Sequestrations, Congenital cystic adenomatoid malformations, and congenital lobar emphysema. Semin Thorac Cardiovasc Surg. 2004;16(3):209-14, http://dx.doi.org/10.1053/j.semtcvs.2004.08.007.
2. Corbett HJ, Humphrey GM. Pulmonary sequestration. Paediatr Respir Rev. 2004;5(1):59–68, http://dx.doi.org/10.1016/j.prrv.2003.09.009.
3. Savic B, Birtel FJ, Tholen W, Funke HD, Knoche R. Lung sequestration: report of seven cases and review of 540 published cases. Thorax. 1979; 34(1):96–101, http://dx.doi.org/10.1136/thx.34.1.96.
4. Wilson RL, Lettieri CJ, Fitzpatrick TM, Shorr AF. Intralobular bronchopulmonary sequestrations associated with bronchogenic cysts. Respir Med. 2005;99(4):508–10, http://dx.doi.org/10.1016/j.rmed.2004.08.014.
5. Stocker JT, Malczak HT. A study of pulmonary ligament arteries: relationship to intralobar pulmonary sequestration. Chest. 1984;86(4): 611-5, http://dx.doi.org/10.1378/chest.86.4.611.
6. Lee EY, Boiselle PM, Cleveland RH. Multidetector CT evaluation of congenital lung anomalies. Radiology. 2008;247(3):632-48, http://dx.doi.org/10.1148/radiol.2473062124.
7. Stocker JT, Kagan-Hallet K. Extralobar pulmonary sequestration: analysis of 15 cases. Am J Clin Pathol. 1979;72(6):917-25, http://dx.doi.org/10.1093/ajcp/72.6.917.
8. Felker RE, Tonkin IL. Imaging of pulmonary sequestration. AJR Am J Roentgenol. 1990;154(2):241-9, http://dx.doi.org/10.2214/ajr.154.2.2105007.
9. Frazier AA, Rosado de Christenson ML, Stocker JT, Templeton PA. Intralobar sequestration: radiologic-pathologic correlation. RadioGraphics. 1997;17(3): 725–45, http://dx.doi.org/10.1148/radiographics.17.3.9153708.
10. Wei Y, Li F. Pulmonary sequestration: a retrospective analysis of 2625 cases in China. Eur J Cardiothorac Surg. 2011;40(1):e39–42, http://dx.doi.org/10.1016/j.ejcts.2011.01.080.
11. Huang XY, Xu XM, Yu C, Fan R, Lu YY, Lu SS, et al. Pulmonary sequestration with tuberculosis confined to the sequestrated lung. Ann Thorac Cardiovasc Surg. 2012;18(1):51–5, http://dx.doi.org/10.5761/atcs.cr.11.01835.
12. Pikwer A, Gyllstedt E, Lillo-Gil R, Jönsson P, Gudbjartsson T. Pulmonary sequestration–a review of 8 cases treated with lobectomy. Scand J Surgery. 2006;95(3):190–4, http://dx.doi.org/10.1177/145749690609500312.
13. Fumino S, Iwai N, Kimura O, Ono S, Higuchi K. Preoperative evaluation of the aberrant artery in intralobar pulmonary sequestration using multidetector computed tomography angiography. J Pediatr Surg. 2007; 42(10):1776–9, http://dx.doi.org/10.1016/j.jpedsurg.2007.07.028.
14. Lee EY, Siegel MJ, Sierra LM, Foglia RP. Evaluation of angioarchitecture of pulmonary sequestration in pediatric patients using 3D MDCT angiography. AJR Am J Roentgenol. 2004;183(1):183–8, http://dx.doi.org/10.2214/ajr.183.1.1830183.
15. Johnson PL, Fishman EK, Duckwall JR, Calhoun PS, Heath DG. Interactive three-dimensional volume rendering of spiral CT data: current applications in the thorax. Radiographics. 1998;18(1):165–87, http://dx.doi.org/10.1148/radiographics.18.1.9460115.
16. Frush DP, Donnelly LF. Pulmonary sequestration spectrum: a new spin with helical CT. Am J Roentgenol. 1997;169(3):679–82, http://dx.doi.org/10.2214/ajr.169.3.9275876.
17. Yue SW, Guo H, Zhang YG, Gao JB, Ma XX, Ding PX. The clinical value of computer tomographic angiography for the diagnosis and therapeutic planning of patients with pulmonary sequestration. Eur J Cardio-Thorac. 2013;43(5):946–51, http://dx.doi.org/10.1093/ejcts/ezs484.
18. Yucel O, Gurkok S, Gozubuyuk A, Caylak H, Sapmaz E, Kavakli K, et al. Diagnosis and surgical treatment of pulmonary sequestration. Thorac Cardiovasc Surg. 2008;56(3):154–7, http://dx.doi.org/10.1055/s-2007-965572.
19. Adzick NS, Harrison MR, Crombleholme TM, Flake AW, Howell LJ. Fetal lung lesions: management and outcome. Am J Obstet Gynecol. 1998; 179(4):884–9, http://dx.doi.org/10.1016/S0002-9378(98)70183-8.
20. Tsang FH, Chung SS, Sihoe AD. Video-assisted thoracic surgery for bronchopulmonary sequestration. Interact Cardiovasc Thorac Surg. 2006;5(4):424–6, http://dx.doi.org/10.1510/icvts.2006.128611.
21. Ganeshan A, Freedman J, Hoey ET, Steyn R, Henderson J, Crowe PM. Transcatheter coil embolisation: a novel definitive treatment option for intralobar pulmonary sequestration. Heart Lung Circ. 2010;19(9):561–5, http://dx.doi.org/10.1016/j.hlc.2010.05.008.
22. Chien KJ, Huang TC, Lin CC, Lee CL, Hsieh KS, Weng KP. Early and late outcomes of coil embolization of pulmonary sequestration in children. Circ J. 2009;73(5):938–42, http://dx.doi.org/10.1253/circj.CJ-08-0914.
23. Lee EY, Boiselle PM, Shamberger RC. Multidetector computed tomography and 3-dimensional imaging: preoperative evaluation of thoracic vascular and tracheobronchial anomalies and abnormalities in pediatric patients. J Pediatr Surg. 2010;45(4):811–21, http://dx.doi.org/10.1016/j.jpedsurg.2009.12.013.